



## OPEN ACCESS

## EDITED BY

Yu Zhuang,  
WSL Institute for Snow and Avalanche  
Research SLF, Switzerland

## REVIEWED BY

Zhaowei Ding,  
Chengdu University of Technology, China  
Qiankuan Wang,  
Shanghai Jiao Tong University, China

## \*CORRESPONDENCE

Jinkai Yan,  
✉ yanjinkaisw@163.com  
Zejun Xia,  
✉ 398681761@qq.com

RECEIVED 25 December 2024

ACCEPTED 23 January 2025

PUBLISHED 05 March 2025

## CITATION

Wei G, Xia Z, Yan J, Li B and Wu X (2025)  
Characteristics of landslide movement and  
dynamic processes in Hongyacun landslide  
cluster, Qinghai Province, China.  
*Front. Earth Sci.* 13:1551527.  
doi: 10.3389/feart.2025.1551527

## COPYRIGHT

© 2025 Wei, Xia, Yan, Li and Wu. This is an  
open-access article distributed under the  
terms of the [Creative Commons Attribution  
License \(CC BY\)](https://creativecommons.org/licenses/by/4.0/). The use, distribution or  
reproduction in other forums is permitted,  
provided the original author(s) and the  
copyright owner(s) are credited and that the  
original publication in this journal is cited, in  
accordance with accepted academic practice.  
No use, distribution or reproduction is  
permitted which does not comply with  
these terms.

# Characteristics of landslide movement and dynamic processes in Hongyacun landslide cluster, Qinghai Province, China

Gang Wei<sup>1,2</sup>, Zejun Xia<sup>1,2\*</sup>, Jinkai Yan<sup>3\*</sup>, Bin Li<sup>4,5,6</sup> and Xinning Wu<sup>1,2</sup>

<sup>1</sup>Key Laboratory of Environmental Geology of Qinghai Province, Qinghai Environmental Geological Prospecting Bureau, Xining, Qinghai, China, <sup>2</sup>Qinghai 906 Engineering Survey and Design Institute, Xining, Qinghai, China, <sup>3</sup>Chinese Academy of Geological Sciences, Beijing, China, <sup>4</sup>The Third Non-ferrous Geological Exploration Institute of Qinghai Province, Xining, Qinghai, China, <sup>5</sup>College of Geology and Environment, Xi'an University of Science and Technology, Xi'an, Shaanxi, China, <sup>6</sup>The First Non-ferrous Geological Exploration Institute of Qinghai Province, Xining, Qinghai, China

Landslide clusters pose significant threats to mountainous regions worldwide, with their complex failure mechanisms and dynamic behaviors requiring comprehensive investigation. This study focuses on the Hongyacun landslide cluster in Qinghai Province, China, a representative example of multi-stage slope failures triggered by hydrological and geological interactions. By integrating field observations with advanced numerical modeling, we aim to reconstruct the full kinematic process of four sub-landslides within the cluster and elucidate the critical factors governing their initiation, motion, and deposition. The research provides insights into flow-slide dynamics under rainfall conditions, addressing a key gap in hazard assessment methodologies for analogous landslide-prone regions. A multidisciplinary approach was employed combining detailed field surveys and three-dimensional numerical simulations. Field investigations mapped the spatial distribution and geometric characteristics of the four sub-landslides (total volume:  $2.46 \times 10^6 \text{ m}^3$ ), while geotechnical analyses identified moisture-induced strength reduction as a primary destabilization factor. The Landslides Post-Failure 3D (LPF3D) simulator was implemented to reconstruct landslide kinematics under two scenarios: natural (pre-rainfall) and rainfall-saturated states. The simulations incorporated soil rheological parameters, hydrological conditions, and terrain data, with particular attention to fluid-solid interactions during motion. Numerical simulations revealed distinct motion patterns between dry and saturated conditions. Continuous rainfall infiltration increased soil saturation by 18–25%, reducing shear strength while enhancing material fluidity. This hydrological transformation generated significant hydrodynamic effects during sliding, with fluid drag forces amplifying mobility rather than providing resistance. Sub-landslide H2-2 exhibited the most hazardous behavior, achieving peak velocity of 32.5 m/s within 70 s and traveling 700 m—42% farther than dry-state simulations predicted. Deposit patterns from all sub-landslides showed >85% spatial consistency with field observations, validating the model's predictive capability. This study demonstrates that rainfall-induced pore pressure development creates dual destabilization effects: reducing shear resistance

while enabling fluid-mediated lubrication. The paradoxical role of hydrodynamic forces—enhancing mobility through drag-induced momentum transfer rather than damping—explains the exceptional runout distances observed. The H2-2 sub-landslide's predominance in damage potential correlates with its unique geometric positioning and hydrological connectivity within the cluster. These findings advance understanding of multi-landslide interaction mechanisms and provide a validated framework for assessing rainfall-triggered landslide cascades. The LPF3D methodology proves particularly effective for hazard zonation in complex terrain, offering critical inputs for early warning systems and mitigation planning in comparable geological settings.

#### KEYWORDS

landslide cluster, landslide overlay body, instability mechanism, dynamics analysis, LPF3D

## 1 Introduction

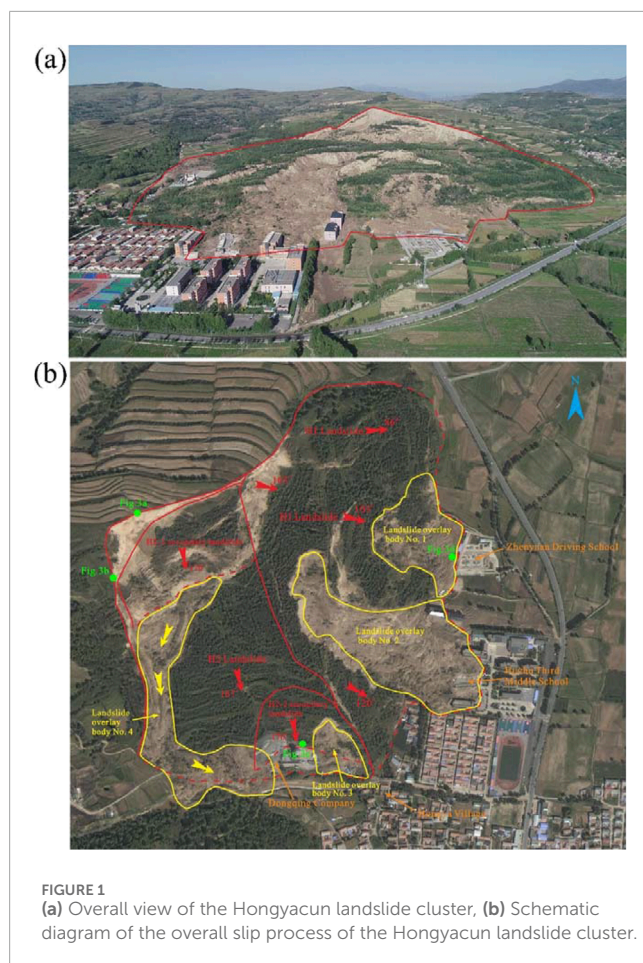
Rainfall is a major factor in triggering flow landslides in mountainous areas. In most mountainous landscapes, landslides may be triggered by either short periods of intense rainfall or long periods of low intensity rainfall (Gao et al., 2017; He et al., 2023; He et al., 2024; Yan et al., 2024). These landslides often occur suddenly and can slide as far as several kilometres at high speeds. In recent years, a number of catastrophic rainfall-induced landslides have occurred in China, resulting in significant casualties and property damage (Yin et al., 2011; Yin et al., 2017; Xing et al., 2015). Therefore, an in-depth understanding of the possible mechanisms and behaviours of these high-level remote landslides from initiation to final deposition is of utmost importance. In order to predict the motion trajectories of landslides after destruction, researchers have developed a variety of dynamic models. For example, a model of a sled (Sassa, 1988), continuum models (Hungri, 1995), quasi-three-dimensional model (Chen and Lee, 2003), continuum medium model of a flow landslide (Crosta et al., 2003), depth-averaged computational model (Denlinger and Iverson, 2004), depth-averaged model for the simulation of rapid landslide motion across complex 3D terrain (McDougall and Hungri, 2004), the continuum mechanics model, RASH3D (Pirulli and Mangeney, 2008), continuum mechanics versus discontinuum mechanics models (Poisel et al., 2008), smoothed particle hydrodynamics (Huang et al., 2012), models considering friction base shear stress, effective coulomb friction coefficient and hypermobility function (Pudasaini and Miller, 2013), SPH depth-integrated model (Pastor et al., 2014), two-dimensional Savage-Hutter model considering velocity-decaying friction law (Liu et al., 2015). Although the validity of these dynamic models has been verified by inverse analyses of several real landslide cases, relatively few reports have successfully predicted landslide motions, mainly because different types of landslides require different models or parameters. However, inversion analysis of cases is still crucial as successful inversion can be used not only to calibrate the model and improve the prediction accuracy, but also to provide specific parameters for similar types of landslides, which can be used for predictive modelling of potential landslides.

There are several numerical simulation software available that have been used in an attempt to better understand and better predict

the mobility of such landslides, these include DAN-W/DAN3D, LS-RAPID, SPH, RAMMS, and others (Hungri, 1995; Hungri and Evans, 2004; Hungri, 2008; Davies and McSaveney, 1999; Xu et al., 2010; Sassa et al., 2010; Tang et al., 2011; Zhang et al., 2010; Xing et al., 2015; Wang et al., 2024). Landslides post failure 3D (LPF3D) is a 3D post landslide numerical simulation software based on a physical model of particle flow regime. It combines the smooth particle hydrodynamics (SPH) method coupled with DEM, FEM, and SDPH to form a new multiphase multimedial numerical simulation method, which is specialised in dealing with the complex interactions of fluids, particles and solids in landslides. This method solves the deficiencies of the traditional methods in computational pressure, accuracy and macroscopic properties acquisition, as well as the difficulties of the Eulerian grid method in landslide trajectory tracking and 3D computation (Gao et al., 2023; Gao et al., 2024a). LPF3D has a wide range of application value in the fields of landslide impacts, engineering protection, geohazard chain, and debris flows due to its high efficiency and accuracy.

At 01:05 on 1 September 2022, a serious landslide occurred in Hongya Village, located in Weiyuan Town, Huzhu County, Qinghai Province, China. The landslide caused damage to several buildings and resulted in seven deaths. Observations showed that the Hongyacun landslide underwent three consecutive sliding processes, resulting in four distinct landslide overlay bodies. After instability of the landslide, long-distance flow sliding occurred, exhibiting the distinctive features of cluster, chain and long-distance sliding. These features make the Hongyacun landslide highly representative of the eastern part of Qinghai, and provide an important case for the study of geological hazards.

In this study, we describe the motion characteristics of the Hongyacun landslide. By analysing the field investigation data, remote sensing interpretation data and rainfall information, we study the destabilisation mechanism of the Hongyacun landslide. LPF3D numerical simulation software was used to simulate the dynamic process of the landslide and to analyse the dynamic mechanism of the landslide. This study not only provides a scientific basis for the causes of Hongyacun landslides, but also provides guidance for the risk assessment and prevention of geological disasters in the region.



## 2 Characteristics of Hongyacun landslide

### 2.1 Sliding characteristics of Hongyacun landslide

The Hongyacun landslide is located in Hongya Village, Huzhu County, eastern Qinghai Province. The geographic coordinates of the centre point of the landslide are  $101^{\circ}56'3.00''\text{E}$ ,  $36^{\circ}51'41.04''\text{N}$ . The location of the landslide is shown in Figures 1, 2. At 16:00 on 31st August, 2022, deformation and sliding occurred in the slope at the back side of the Zhenyuan Driving School in Huzhu County (Figure 1A). At 1:05 on 1 September, another large-scale slide occurred in the landslide area, killing seven people and damaging a large number of buildings, including the teaching building, teachers' apartment and laboratory building of the Third Middle School in Huzhu County, the villagers' houses in the Hongya villages, as well as the plant facilities of the Zhenyuan Driving School and the Dongqing Concrete Company Limited. The direct economic loss was 85.51 million yuan.

The Hongyacun landslide slid three times successively, forming four landslide overlay bodies. on August 31, the first landslide occurred on the back side of Zhenyuan Driving School, the landslide debris flow slid a distance of about 75 m, burying the colourful steel room of Zhenyuan Driving School and forming No. 1 landslide

overlay body. At 1:05 a.m. on September 1, the slope on the back side of the Huzhu Third Middle School slid as a whole to the school area below, with a slip distance of 210 m, buried the school below, resulting in the destruction of three school buildings, seven people died, the formation of No.2 and No.3 landslide overlay bodies. At the same time, the slip unloading in the centre-front part of the landslide led to destabilisation and deformation in the centre-back part of the slide. As the slope was in a high water content state, this part of the slide formed a fluvial landslide, which partly overtopped to the opposite slope, forming a rung terrain. Most of the slide body slid downward along the right side of the gully for about 460 m, burying part of the plant on the west side of Dongqing Concrete Company Limited, forming the No.4 landslide overlay body. The sequence of the whole sliding process is as follows: No. 1 landslide overlay body → No. 2 and No. 3 landslide overlay bodies → No. 4 landslide overlay body. Figure 1B shows the schematic diagram of the overall sliding process of the landslide.

### 2.2 Morphological characteristics of Hongyacun landslide cluster

Hongyacun landslide cluster is developed in the transition zone between low hills and river valley plains. The overall shape of the landslide resembles a 'wide tongue', and the main slip direction is ranges between  $103^{\circ}\sim 167^{\circ}$ . The elevation of the trailing edge is 2,666~2726 m, the elevation of the front edge is 2,547~2580 m, and the overall elevation difference is 114~152 m. The longitudinal length of the landslide is about 370~740 m, the transverse width is about 470~1050 m, and the area is about  $53.2 \times 10^4 \text{ m}^2$ . The average thickness of the body of the landslide is about 40 m, and the total volume is about  $2,108 \times 10^4 \text{ m}^3$ , which is an exceptionally large landslide. The boundary of the landslide is clear, the trailing edge of the slide wall extension length of about 480 m, was arc-shaped steep elevation, slope  $60 \sim 70^{\circ}$ , the height of the slide wall 8 ~ 40 m. The west side of the shear side wall extension length of about 255 m, was arc-shaped steep elevation, slope  $70^{\circ}$  or so, the side wall height of 13 ~ 21 m. The east side of the landslide in the natural ditch as a boundary, the east side of the boundary of the leading edge of the shear exit is located in the foot of the slope terraced junction parts, shear exit is manifested as a series of dropsy deformation. In the west side of the Dongqing concrete mixing plant, the back side of the residential area of Hongya Village, Zhenyuan Driving School to the north and other areas can be seen in the obvious signs of ground uplift and dropsy, the terrain displacement is obvious. The basic situation of the Hongyacun landslide is shown in Figure 1B.

According to the spatial morphology, main slide direction and structural characteristics of the landslide cluster, the Hongyacun landslide cluster can be divided into two main sliding areas, i.e., landslide H1 and landslide H2. Landslide H2 contain two secondary landslides, namely, secondary landslide H2-1 and secondary landslide H2-2. As a result of remote sliding of the landslides, two landslide overlay body were formed on the H1 landslide, namely, No. 1 and No. 2, and two landslide overlay body were formed on the H2 landslide, namely, No. 3 and No. 4, as shown in Figure 1B.



**FIGURE 2** Basic characteristics of hongyaacun landslide. **(a)** Bank wall of the landslide **(b)** sidewall of the landslide **(c)** bulge at the leading edge **(d)** bulge at the leading edge.

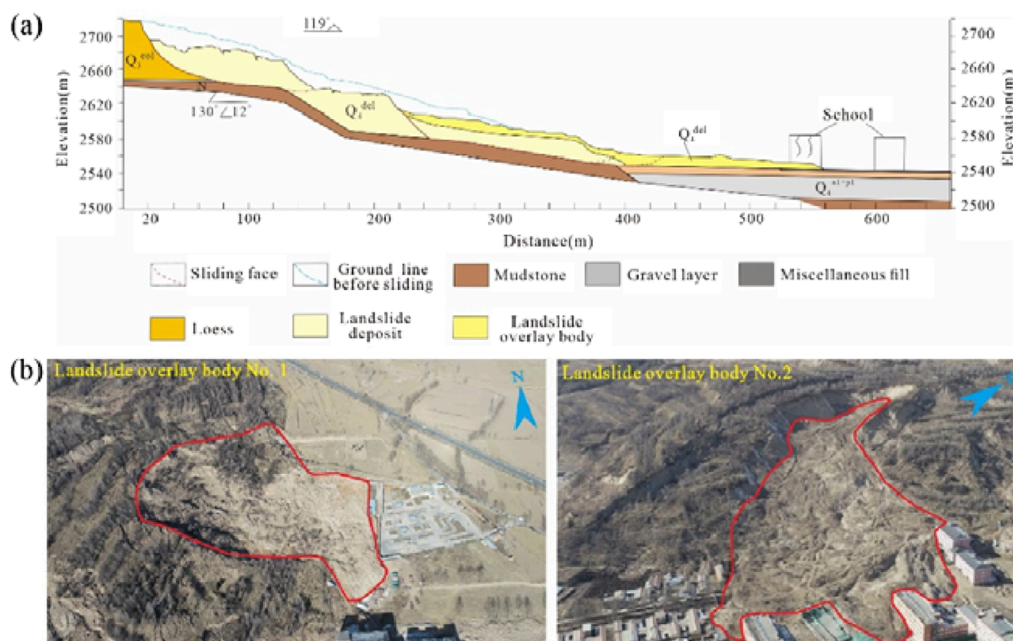


**FIGURE 3** **(a)** H1 landslide profile of hongyaacun landslide, **(b)** Full view of landslide overlay body No. 1 and No. 2 of landslide H1 of Hongyaacun Landslide.

### 2.2.1 H1 landslide of Hongyaacun landslide

H1 landslide is located in the east side of the Hongyaacun landslide, the plan form is “wide tongue” shape, with a main slip direction 103 ~ 120°. The back edge elevation 2,692 ~ 2710 m, the front edge elevation 2,546 ~ 2562 m, the overall drop of about 130 ~ 165 m. The longitudinal length is 410~740 m, the transverse width is 200~900 m, the area is  $31.7 \times 10^4 \text{ m}^2$ , the average thickness of the slide body is 40 m, and the volume is  $1,268 \times 10^4 \text{ m}^3$ . the terrain of the landslide is high in the west and low in the east, and the slope degree is 16°~20°, and the sliding form multi-levels. After

sliding, it formed multi-stage platform, and the overall displacement amounted to 52 m. After sliding, the terrain was broken, undulating and uneven, and 2 levels of obvious downward sliding walls were developed, which were located in the rear edge and the middle part. After the landslide, more anti-slopes and depressions were formed in the rear and central part of the landslide, and a stacked-tile topography was formed in the rear edge. Shear walls and cracks on the slope are more developed, and there are more steep cliffs, broken walls and pull-down slots, the height of steep cliffs and broken walls is generally 3–5 m, and the depth of pull-down slots

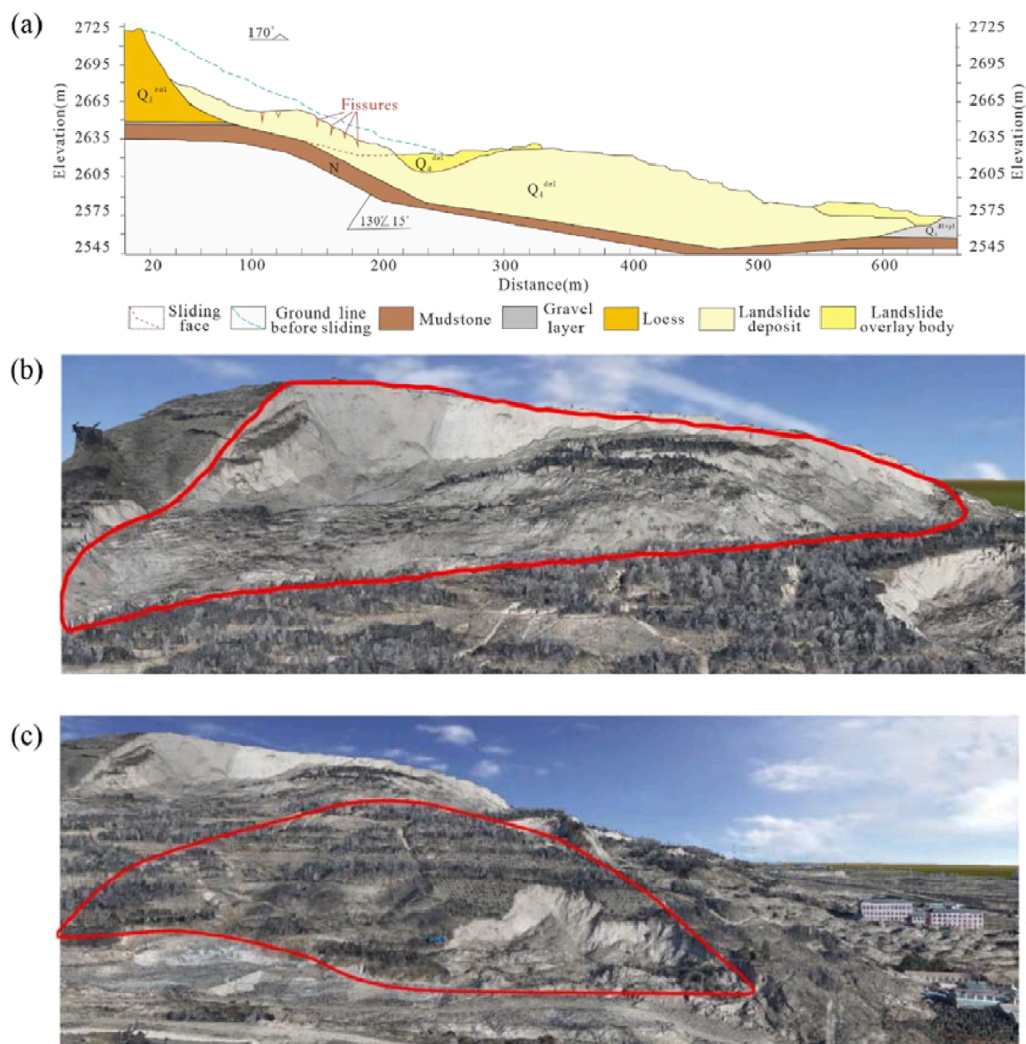


FIGURE 4  
(a) H2 landslide profile of the Hongyaacun landslide, (b) Full view of H2-1 secondary landslide, (c) Full view of H2-2 secondary landslide.

is generally 2–4 m, and the width is 3–5 m. H1 landslide profile is shown in Figure 3A.

The front slide of landslide H1 has been sliding remotely, and two landslide overlay bodies have been developed. The No. 1 landslide overlay body is located at the back side of Zhenyuan Driving School, with irregular “dustpan” shape, length of landslide overlay body about 120 m, width of landslide overlay body 110 m, average thickness of landslide overlay body about 8 m. The main direction of sliding is 103°, area of landslide overlay body is  $3.67 \times 10^4 \text{ m}^2$ , the volume of landslide overlay body is  $29.3 \times 10^4 \text{ m}^3$ , movement distance about 75 m. The No.2 landslide overlay body is located in the back side of Huzhu Third Middle School, the plan form is of a “long tongue” type, the average length of the landslide overlay body is about 320 m, the average width is about 120 m, the average thickness is about 8 m, the main sliding direction is 108°, the slip cover area is  $7.8 \times 10^4 \text{ m}^2$ , and the volume is  $62.4 \times 10^4 \text{ m}^3$ . The difference in elevation between front and back of the No.2 landslide overlay body is big, and the shear exit position is higher. The slide

body high-speed remote slip, slip distance up to 210 m, as shown in Figure 3B.

### 2.2.2 H2 landslides in the hongyaacun landslide

H2 landslide is located in the southwest side of the Hongyaacun landslide, the plan form is ‘long tongue’ shape, the main slip direction of about 167°. The elevation of the back edge is 2,710–2,728 m, the elevation of the front edge is 2,554–2,580 m, and the overall difference in elevation is about 140–155 m. The longitudinal length of the landslide is about 600 m, the transverse width is 300–500 m, the area is about  $21 \times 10^4 \text{ m}^2$ , and the average thickness of the landslide body is about 40 m, and the volume is  $840 \times 10^4 \text{ m}^3$ . The terrain is high in the north and low in the south, with an overall slope of 16°–20°, the rear H2-1 secondary landslide is higher than the front H2-2 secondary landslide by 20–40 m, with a slip of up to 45 m, and the slope is basically disintegrated after it is situated, and the slope of the rear edge is stacked tile-like, with a slope of about 5°–10°, and locally there are ring-type



FIGURE 5 Full view of landslide overlay bodies No. 3 and No. 4.

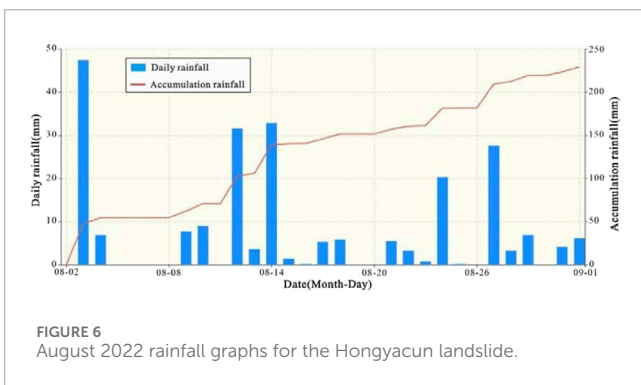


FIGURE 6 August 2022 rainfall graphs for the Hongyacun landslide.



FIGURE 7 Development of drop holes on landslide mass.

grooves and strip landslide depressions, the front edge of the H2-1 secondary landslide is steeper, with a slope of 40°–45°, forming good free surface conditions. The displacement of the slope body in the middle and front part of the H2 landslide is not large, and the slope body disintegration is not obvious, basically maintaining

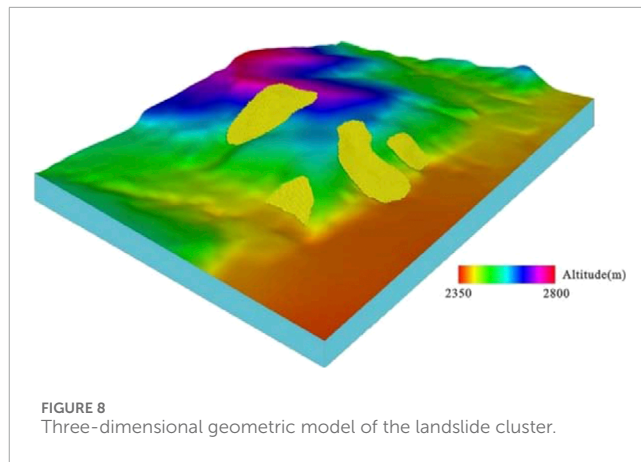


FIGURE 8 Three-dimensional geometric model of the landslide cluster.

the original slope condition. The cross-section of the H2 landslide is shown in Figure 4A.

H2-1 secondary landslide is located at the rear of H2 landslide, the back edge and both sides of the boundary basically coincide with the H2 landslide, and the shear exit is located in the centre of the platform at the turn. The elevation of the back edge ranges from 2,680 to 2,706 m, and the elevation of the shear exit is between 2,619 and 2,640 m, and the overall elevation difference is 60–70 m. H2-1 secondary landslide is in the form of a ‘rectangle’, with the main slip direction of about 170°, an area of about  $4.56 \times 10^4 \text{ m}^2$ , an average thickness of the slide body of about 21 m, and a volume of about  $96 \times 10^4 \text{ m}^3$ , as shown in Figure 4B.

H2-2 secondary landslide is located at the front edge of H2 landslide, with a rear elevation ranging from 2,610 to 2,615 m and a shear elevation between 2,561 and 2,566 m, resulting in an overall elevation difference of 46–55 m. The landslide platform is in the shape of ‘tongue’, the main slip direction is about 163°, the area is about  $3.06 \times 10^4 \text{ m}^2$ , the average thickness is about 19 m, the volume is  $58 \times 10^4 \text{ m}^3$ , and the material composition of the landslide is loess and fractured mudstone, as shown in Figure 4C.

H2 landslide developed two landslide overlay bodies. Among them, the No. 3 landslide overlay body is located in the east side of Dongqing Concrete Co., Ltd., the plane form is irregular ‘tongue’, the landslide overlay body is about 120 m long, 110 m wide, average thickness is about 5 m, the main slip direction is 170°, the landslide overlay body area is  $1.2 \times 10^4 \text{ m}^2$ , the volume is about  $6 \times 10^4 \text{ m}^3$ . The slide body as a whole slid down, the movement distance of about 60 m, destroyed the east side of Dongqing Concrete Company Limited part of the plant and vehicles. The No.4 landslide overlay body is located in the west of Dongqing Concrete Co., Ltd., and its plan form is ‘irregular’, the No.4 landslide overlay body is blocked by the mountain, and its movement direction has been turned several times, the rear transport direction is about 223°, the middle transport direction is about 177°, and the front transport direction is about 104°. The axial extension of the landslide overlay body is about 700 m long, 50–90 m wide on average, 10 m thick on average, with an area of  $5.8 \times 10^4 \text{ m}^2$  and a volume of  $58 \times 10^4 \text{ m}^3$ . The material of No.4 landslide overlay body mainly comes from H2-1 secondary landslide, the original topography and bedrock surface of the location where the landslide is located

TABLE 1 Parameters of LPF3D simulation of Hongyacun landslide.

Serial number	Working condition	Particle phase			fluid phase	
		density (kg/m <sup>3</sup> )	Coefficient of friction	pore water pressure factor	density (kg/m <sup>3</sup> )	Coefficient of viscosity (Pa·s)
Nos. 1, 2, 3 and 4	nature	1700	0.7	0	—	—
	rainfall	1700	0.2	0.3	1,200	0.0015

are steeper, the slip body of H2-1 secondary landslide is sheared out in the middle, and part of it is washed over to the opposite slope, forming a Longang terrain, and most of the slip body is transported downward at high speed of about 460 m along the gully, and the tongue of the slip is covered by the part of the plant on the west side of Dongqing Concrete Company Limited, as shown in Figure 5.

## 3 Analysis of triggering factors of Hongyacun landslide

### 3.1 Geological environment factors

The Hongyacun landslide is located in the eastern part of Qinghai Province, at the westernmost end of the Loess Plateau, which is the area with the most significant loess development in Qinghai Province. The region has been subjected to strong geological effects, and its geomorphological features show the characteristics of interlocking gullies and ravines, forming a variety of loess geomorphological units and a large number of loess gullies and valleys. Influenced by internal or external forces, either alone or jointly, erosion and damage, steep terrain appears widely on both sides of rivers, gullies, highways, railways, etc., which provides good proximity conditions for the formation of loess landslide clusters.

The overall height difference of the landslide cluster of Hongyacun is about 150 m, the average slope is about 20°, and the slope in local area is as high as 50°–60°. The steep topography provides favourable free surface conditions for the formation of the landslide cluster. In addition, the lithology of the landslide body is the wind-deposited loess (Q<sub>3</sub><sup>col</sup>) of the Upper Pleistocene, with a loose structure and developed vertical joints and fissures, which is the material basis for the occurrence of landslides. And the lower part of loess, the Neoproterozoic mudstone becomes the key structural surface to control the landslide. Moreover, the overall slope direction of the landslide is 120°–170°, and the stratigraphy of the underlying mudstone has an inclination of 130°, with a dip angle of 12°–15°, which is a downward slope, providing favourable geological conditions for the sliding of the landslide body, and the soft and weak interlayers in the mudstone provide mechanical conditions for the downward sliding of the landslide.

In the rear part of the landslide, there is an upper layer of stagnant water in the gravel layer at the bottom of loess. At the

same time, the area is rich in groundwater, groundwater long-term recharge to the landslide area, causing a saturated silt layer at the bottom of the loess in the landslide area, and the bedrock weathering fissure zone has been in a state of water saturation for a long time. The long-term action of groundwater not only reduces the strength of loess and mudstone, forming a weak sliding surface, but also the buoyancy force and drag force formed by the dynamic water pressure of groundwater are important factors leading to landslide sliding (Gao et al., 2022).

At the foot of the landslide, there are residential areas, the Huzhu Third Middle School, a brick factory, a driving school and a concrete mixing plant, among other infrastructures. These facilities in the construction of the foot of the slope generally cut the slope treatment, the formation of the height of about 4–40 m ranging from steep slopes, the gradient of 50 ~ 80°. Excavation of the foot of the slope not only changed the stress state of the leading edge slope, but also greatly reduced the slip resistance of the foot of the slope. Excavation of the foot of the slope is also an important factor in inducing landslides.

In addition, on the surface of the landslide, there are greening and irrigation works. These works have a grid-like underground pipe network and locally constructed cisterns with localised water leakage. The irrigation and landscaping works increased the water content of the landslide, leading to an increase in heaviness and softening of the soil, which triggered the localised landslides.

In summary, the influence of geological environment on the development of landslides is manifested in many aspects such as topography and geomorphology, stratigraphic lithology, groundwater and so on, which are the basis of the development of landslides and intrinsic factors of landslide development.

### 3.2 Rainfall factors

Continuous heavy rainfall in August was an important triggering factor for the Hongyacun landslide. According to monitoring data from nearby rainfall stations (Figure 6), eight rounds of heavy rainfall processes were experienced in August, with a cumulative total of 21 days of rainfall and a total rainfall of 224.7 mm. Among them, the maximum 24-h rainfall was recorded on August 3, amounting to 47.4 mm. The cumulative rainfall for the 5 days prior to the landslide (27–31 August) totaled to 41.8 mm. On the one hand, rainfall infiltration causes the soil body's self-weight to increase, making the sliding force larger. On the other hand, the potential slip surface becomes saturated, weakening its mechanical properties and reducing the slip resistance. Additionally, rainfall infiltration recharge causes the

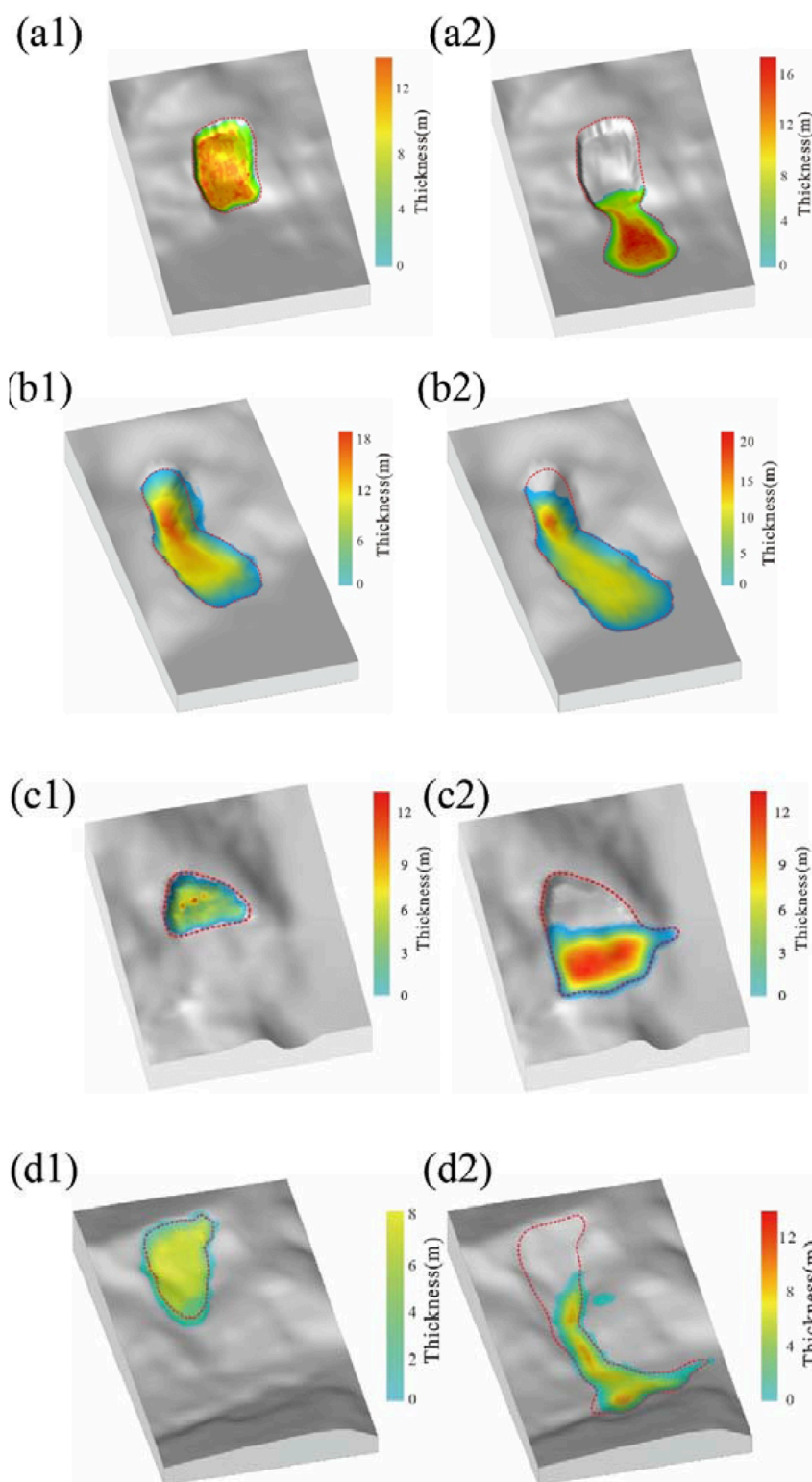


**FIGURE 9** Comparison of the results of the movement and accumulation of different landslide overlay body under different working conditions. **(a1)** No. 1 landslide overlay body under the natural working conditions (stack thickness 12 m), **(a2)** No. 1 landslide overlay body under rainfall conditions (stack thickness 14 m), **(b1)** No. 2 landslide overlay body under the natural working conditions (stack thickness 18 m), **(b2)** No. 2 landslide overlay body under the natural working conditions the rainfall conditions (stack thickness 20 m), **(c1)** No. 3 landslide overlay body under the natural working conditions (stack thickness 10 m), **(c2)** No. 3 landslide overlay body under the rainfall conditions (stack thickness 20 m), **(d1)** No. 4 landslide overlay body under the natural working conditions (stack thickness 10 m), **(d2)** No. 4 landslide overlay body under the rainfall conditions (stack thickness 10 m).

TABLE 2 Simulation results of landslide overlay body motion velocity.

	Sliding duration(s)	Peak velocity (m/s)
No. 1 landslide overlay body	40	22.4
No. 2 landslide overlay body	60	21.8
No. 3 landslide overlay body	30	18.5
No. 4 landslide overlay body	70	32.5

groundwater level to rise rapidly within the slide, leading to a sharp increase in dynamic water pressure and mudstone fissure water bearing pressure. This forms a strong “buoyant force” at the bottom of the slip surface, resulting in a decrease in the normal pressure at the front of the landslide’s slip resistance section. Consequently, the friction force between the slide and the sliding bed of the body decreases dramatically, ultimately triggering the overall slip of the landslide. The slide will eventually be triggered to slide as a whole.

According to the field investigation, the landslide body has many drop holes (Figure 7), and the total number of drop holes developed in the back edge and the centre is about 20. The diameters of the drop holes range is 1–3 m, and some of the drop holes are connected at the bottom to form surface collapses, with a collapse length of more than 20 m and a width of 5 m. The existence of these drop holes provides a natural infiltration channel for rainfall, which can rapidly enter the slope and reach the water barrier layer, leading to a rapid reduction in the shear strength of the potential slip surface and triggering sliding damage.

## 4 Analysis of landslide dynamic processes

### 4.1 Numerical simulation method and calculation process

#### 4.1.1 Introduction of the method

The Landslides post failure 3D (LPF3D) numerical simulation software derives its theoretical basis from a complex particle flow physics model. By integrating the Smooth Particle Hydrodynamics (SPH) method, a coupling bridge with DEM, FEM, SDPH and other methods is successfully constructed, thus pioneering a new numerical simulation method for multiphase multimedial coupled computation, which is specifically designed to deal with the complex interactions of landslide fluids, granular bodies and solids. Compared with software focused on continuous media simulation such as DAN-W (Yin et al., 2016) and RAMMS (Zhang et al., 2023), and discrete element software PFC (Zhang et al., 2020), which focuses on particle flow simulation, LPF3D is able to deal with these different physical phases in a unified framework, showing its unique advantages (Gao et al., 2024b).

This method not only effectively overcomes the computational pressure, lack of accuracy and difficulty in obtaining the macroscopic properties of the system when dealing with a large amount of data using the traditional discrete cell method, but also solves the technical difficulties of the traditional Eulerian grid method in tracking the trajectory of landslide motion and realising the full three-dimensional computation (Gao et al., 2023; Gao et al., 2024a). With its efficient and high-precision computational capability, LPF3D is widely used in the solution of complex dynamics problems such as landslide dynamics protection engineering, high-speed remote landslide impact scavenging, geological disaster chain blocking river and dam break, and two-phase flow motion of debris flow.

#### 4.1.2 Calculation method

The computational method used in this software is the macroscopic continuous medium algorithm, which is applicable to the computation of discrete granular materials and fluid-mediated materials, all based on the continuity equation (Equation 1), the equation of motion (Equation 2), and the energy equation (Equation 3) of hydrodynamics (Gao et al., 2023; Gao et al., 2024b). When dealing with granular objects such as gravel, sand and soil involved in landslide motion, the smooth discrete particle hydrodynamics approach is used for modelling and solution. This method ensures the rigour, stability and accuracy of the calculations and provides a reliable mathematical basis for the simulation of the landslide motion process.

$$\frac{dp_i}{dt} = \sum_{j=1}^N m_j v_j \cdot \nabla_i W_{ij} \quad (1)$$

$$\frac{dv_i}{dt} = - \sum_{j=1}^N m_j \left( \frac{\sigma_i}{\rho_i^2} + \frac{\sigma_j}{\rho_j^2} + \Pi_{ij} \right) \nabla_i W_{ij} - \frac{\nabla P}{\rho_p} + \mathbf{g} + \mathbf{R}_{gp}^{rsdph} + \frac{f_i^{bp}}{\rho_i} \quad (2)$$

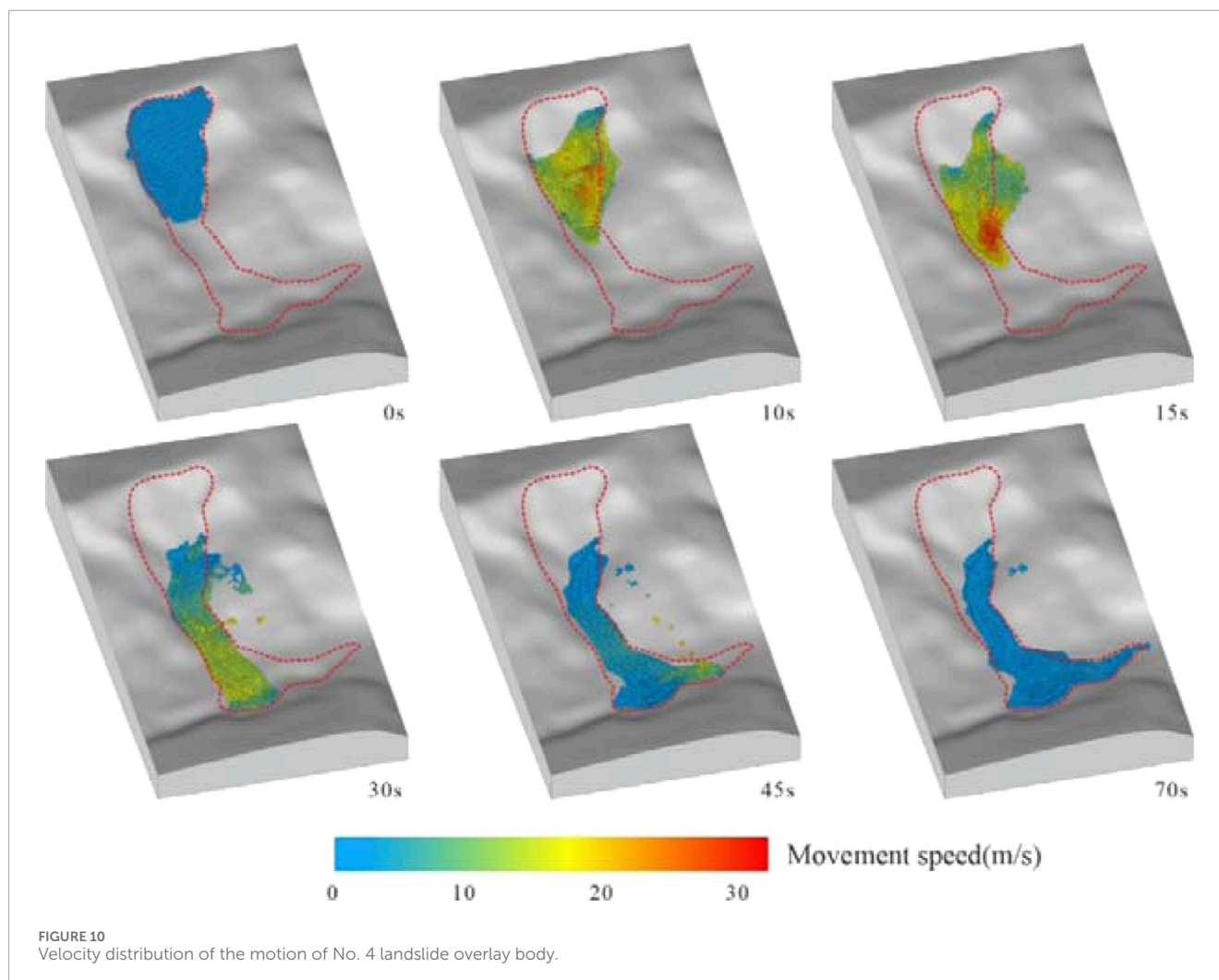
$$\frac{d\theta_{pi}}{dt} = \frac{2}{3} \left( \frac{1}{2} \sum_{j=1}^N m_j v_{ji} \left( \frac{\sigma_i}{\rho_i^2} + \frac{\sigma_j}{\rho_j^2} - \Pi_{ij} \right) \nabla_i W_{ij} + \sum_{j=1}^N m_j \left( \frac{k_p(\nabla\theta_p)_i}{\rho_i^2} + \frac{k_p(\nabla\theta_p)_j}{\rho_j^2} \right) \nabla_i W_{ij} - N_c \theta_{pi} - \varphi_{gp} \right) \quad (3)$$

Each physical quantity is represented by the following symbols:  $\rho_i$  for density,  $v_i$  for velocity,  $e_i$  for energy,  $m_i$  for mass, and  $\sigma_i$  for the stress tensor. The pressure gradient of the continuous phase is denoted by  $\nabla p$  and the pressure gradient of the discrete phase is denoted by  $\nabla P_p$ . External volume forces are denoted by  $\alpha_p \rho_p \mathbf{g}$  and interphase interaction forces are denoted by  $\mathbf{R}_{pg}$ . In addition,  $f_i^{bp}$  represents the boundary force tensor. The energy dissipation term is represented by  $k_p \nabla \theta_p$ , where  $k_p$  is the energy dissipation factor. The energy dissipation term due to inter-particle collisions is denoted by  $N_c \theta_p$ .  $\varphi_{gp}$  is the energy exchange between the continuous and particulate phases and is generally taken as  $\varphi_{gp} = -3\beta_{gp} \theta_p$ , where  $\beta_{gp}$  is the coefficient of trailing force between the fluid phase and the particulate phase.

### 4.2 Model establishment and parameter selection

#### 4.2.1 Numerical model establishment

In order to accurately and quantitatively describe the topographic and geomorphological features of the Hongyacun



landslide cluster, this study used 1:2,000 scale 3D contour data to construct a topographic and geomorphological model of the landslide complex. In the slide source area, loess slide and fluid models were set up respectively, as shown in Figure 8.

Based on the assumption that the landslide was triggered by the impact of continuous rainfall, in order to simulate the process of motion accumulation of fluids and geotechnical particles, inverse simulations were carried out to assess and analyse key quantitative data such as the distance of movement, speed of movement, and accumulation extent of the landslide. The results of these analyses will provide important technical support for the spatial prediction, disaster prevention and mitigation, and emergency relief of loess landslides in eastern Qinghai.

#### 4.2.2 Selection of simulation parameters

The physico-mechanical parameters of the slide material are adopted from the actual parameters, which are basically consistent with the parameters of the real landslide material. The slide material consists of loess with a solid particle density  $\rho = 1,700 \text{ kg/m}^3$ . The fluid material is dilute slurry with main parameter  $\rho = 1,200 \text{ kg/m}^3$  and viscosity coefficient  $0.0015 \text{ Pa}\cdot\text{s}$ . The solid material is simulated by multi-physical state simulation technique of dense, dilute and

ultra-dilute. The volume fraction critical value of the dense and transition states is 60%, and that of the transition and dilute states is 40%. When the volume fraction is less than 2% for the ultra-sparse state, the fluids and solids are simulated using fully coupled numerical simulations with the same location and different volume value assignments. The simulation objects are No.1, No.2, No.3 and No.4 landslide overlay bodies, respectively. The specific simulation parameters are shown in Table 1.

### 4.3 Analysis of simulation results

#### 4.3.1 Comparison of simulation results for different working conditions

The simulation results of the No.1 landslide overlay body are compared and analysed in the natural working condition: the maximum thickness of the landslide overlay body is 12 m, when rainfall is not taken into account, the slip body is a simple dry loess solid, and no fluid coupling is taken into account, and no movement of the slip body occurs. Rainfall conditions: rainfall and loess fully coupled, prompting the slip body instability to start sliding, solid particles in the fluid phase between the drag effect of the formation of long-distance movement,

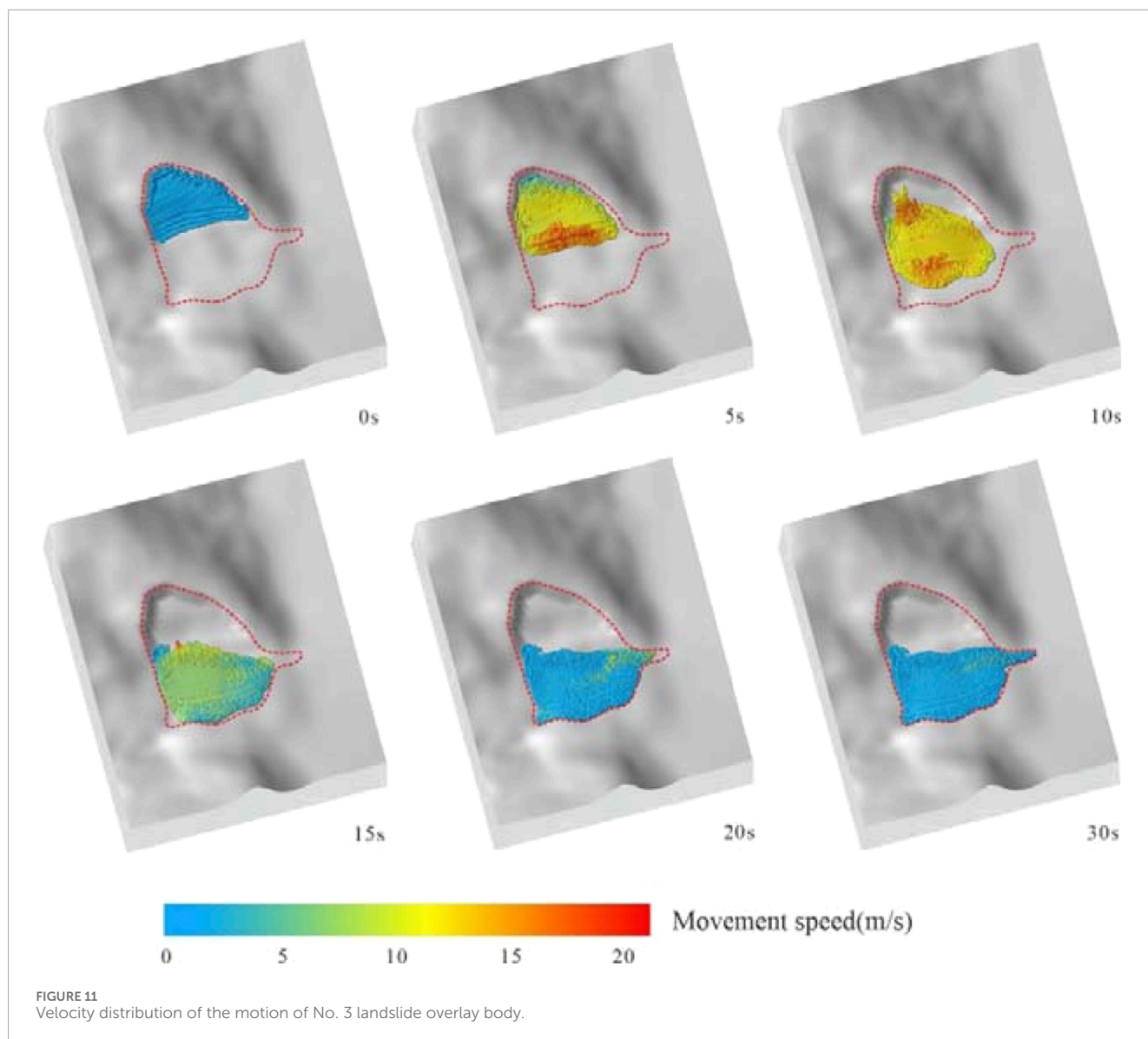


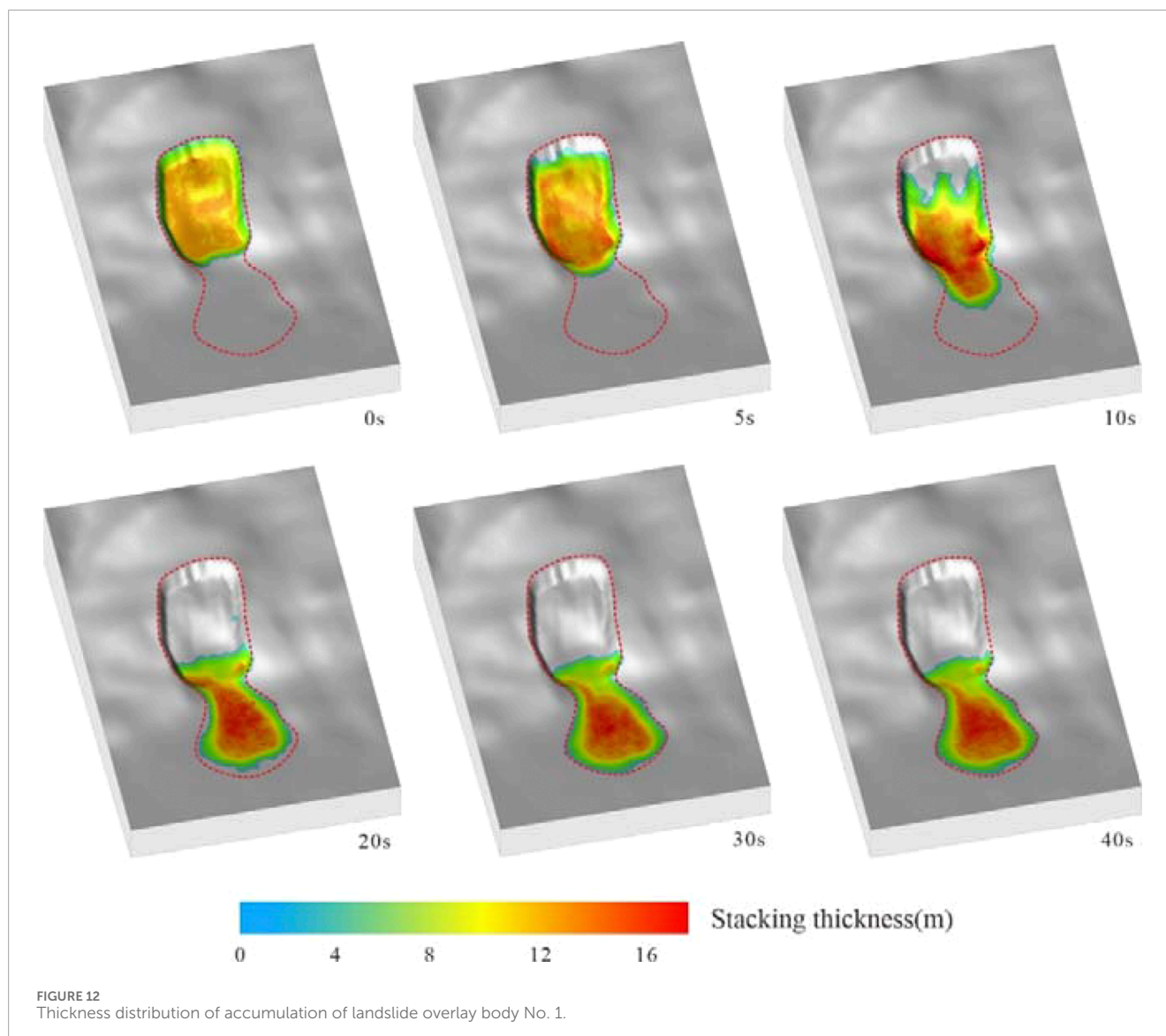
**TABLE 3** Simulation results of the accumulation of the landslide overlay body.

	Maximum movement distance(m)	Peak stack thickness(m)
No. 1 landslide overlay body	300	14
No. 2 landslide overlay body	480	18.5
No. 3 landslide overlay body	200	12
No. 4 landslide overlay body	700	10

with obvious fluidisation characteristics. The maximum thickness of the deposit reached 14 m, and the maximum distance of movement was 300 m. After being cut out along the shear exit, the landslide overlay

body were characterised as sliding in a straight line. During the sliding process, the landslide overlay body consumed energy and eventually piled up to form, and their piled-up morphology showed an irregular skip shape, which was consistent with the piled-up morphology of the No.1 landslide overlay body (Figures 9A1, 9A2).

Comparative analysis of the simulation results of the No.2 landslide overlay body. Natural condition: when rainfall is not considered, the slide is a pure dry loess solid, without considering fluid coupling, the slide is relatively stable, no movement occurs, and the maximum thickness of the slide is 18 m. Rainfall condition: the rock and soil body of the landslide overlay body slides forward under the effect of vibration influenced by rainfall, and the maximum thickness of the accumulation occurs in the foot of the slope, with the maximum thickness of the accumulation reaching 20 m, and the maximum distance of the movement is 480 m. After being sheared out along the shear outlet, the landslide overlay body exhibited linear sliding kinematics, and their final stacking morphology showed a long tongue shape, a feature that matches the stacking morphology of the No.2 landslide overlay body (Figures 9B1, 9B2).

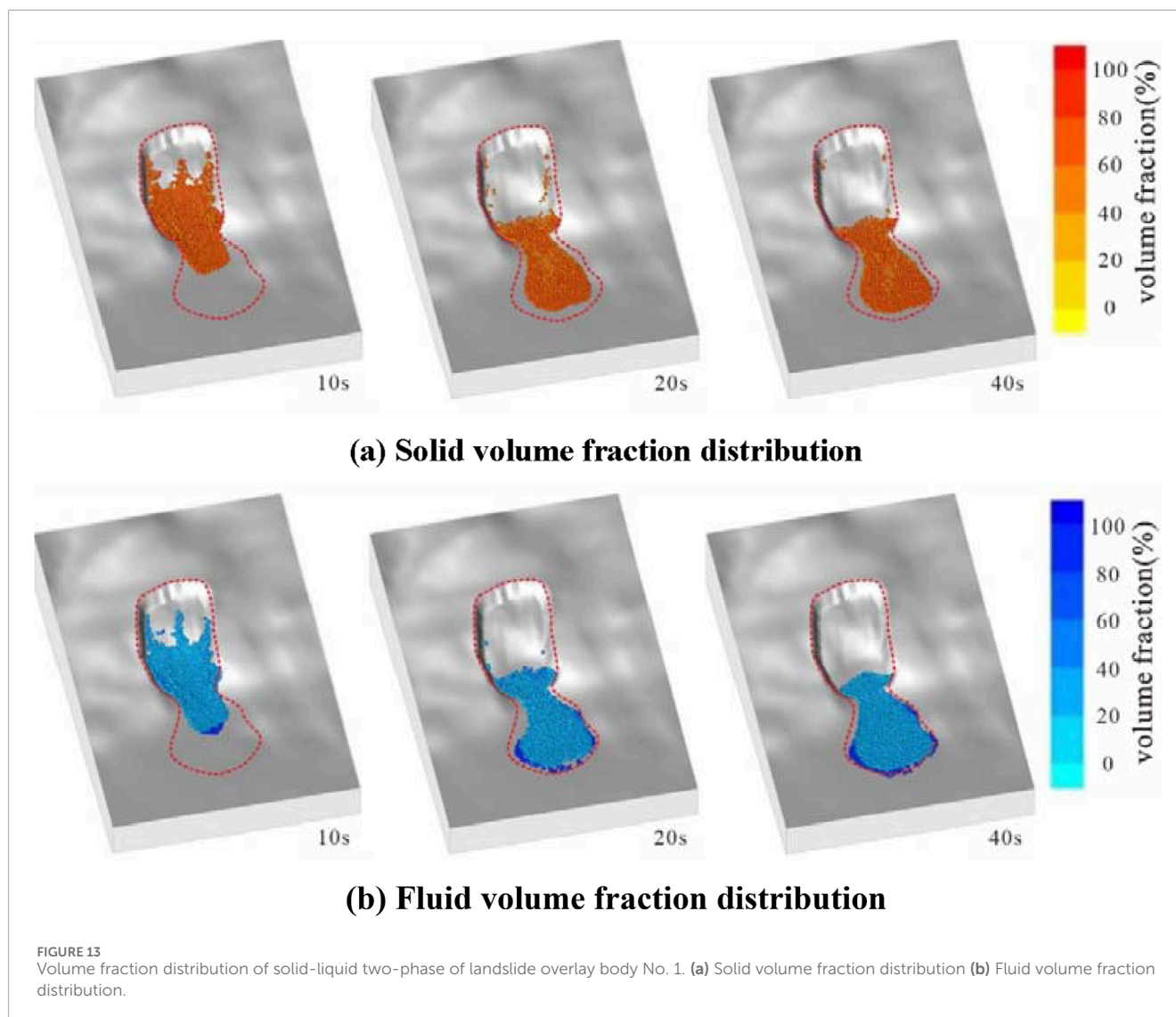


Comparative analysis of the simulation results of the No.3 landslide overlay body. Natural working condition: the maximum thickness of the landslide overlay body is 10 m, when rainfall is not considered, the slip body is pure dry loess solid, fluid coupling is not considered, and no movement of the slip body occurs. Rainfall conditions: rainfall and loess fully coupled, prompting the slip body instability to start sliding, solid particles in the fluid phase between the drag effect of the formation of long-distance movement, with obvious fluidisation characteristics. The maximum accumulation thickness of the stack reached 12 m, and the maximum movement distance was 200 m. After being cut out along the shear outlet, the landslide overlay body undergoes an overall misalignment and piles up at the foot of the slope, and its final stacking pattern takes on a tongue-like shape, a feature that matches the stacking pattern of the No.3 landslide overlay body (Figures 9C1, 9C2).

The maximum thickness of the No.4 landslide overlay body is 8 m, when rainfall is not considered, the slip body is pure dry loess solid, and no fluid coupling is considered, the slip body did

not move. Rainfall conditions: rainfall and loess fully coupled to the case, prompting the slip body instability to start sliding, solid particles in the fluid phase between the drag effect of the formation of long-distance movement, with obvious fluidisation characteristics. The maximum accumulation thickness of the stack reached 10 m, and the maximum movement distance was 700 m. After instability, the direction of movement of the landslide overlay body turned several times because it was blocked by the mountain. Specifically, the rear transport direction was about 223°, the middle transport direction was about 177°, and the front transport direction was about 104°. During the whole movement process, the landslide overlay body showed the characteristic of flow-like sliding. Eventually, its accumulation pattern shows an irregular shape, which is consistent with the accumulation pattern of the No.4 landslide overlay body (Figures 9D1, 9D2).

Comparing the numerical simulation results under different working conditions, it can be found that the presence of fluid under rainfall conditions promotes the movement of the solid, the solid presents multi-physical state changes during



the landslide movement, and the interphase effect of fluid on the solid makes the landslide form a long-distance movement, and the obtained computational results are close to the actual ones.

#### 4.3.2 Analysis of the simulation results of the motion velocity of the landslide overlay body

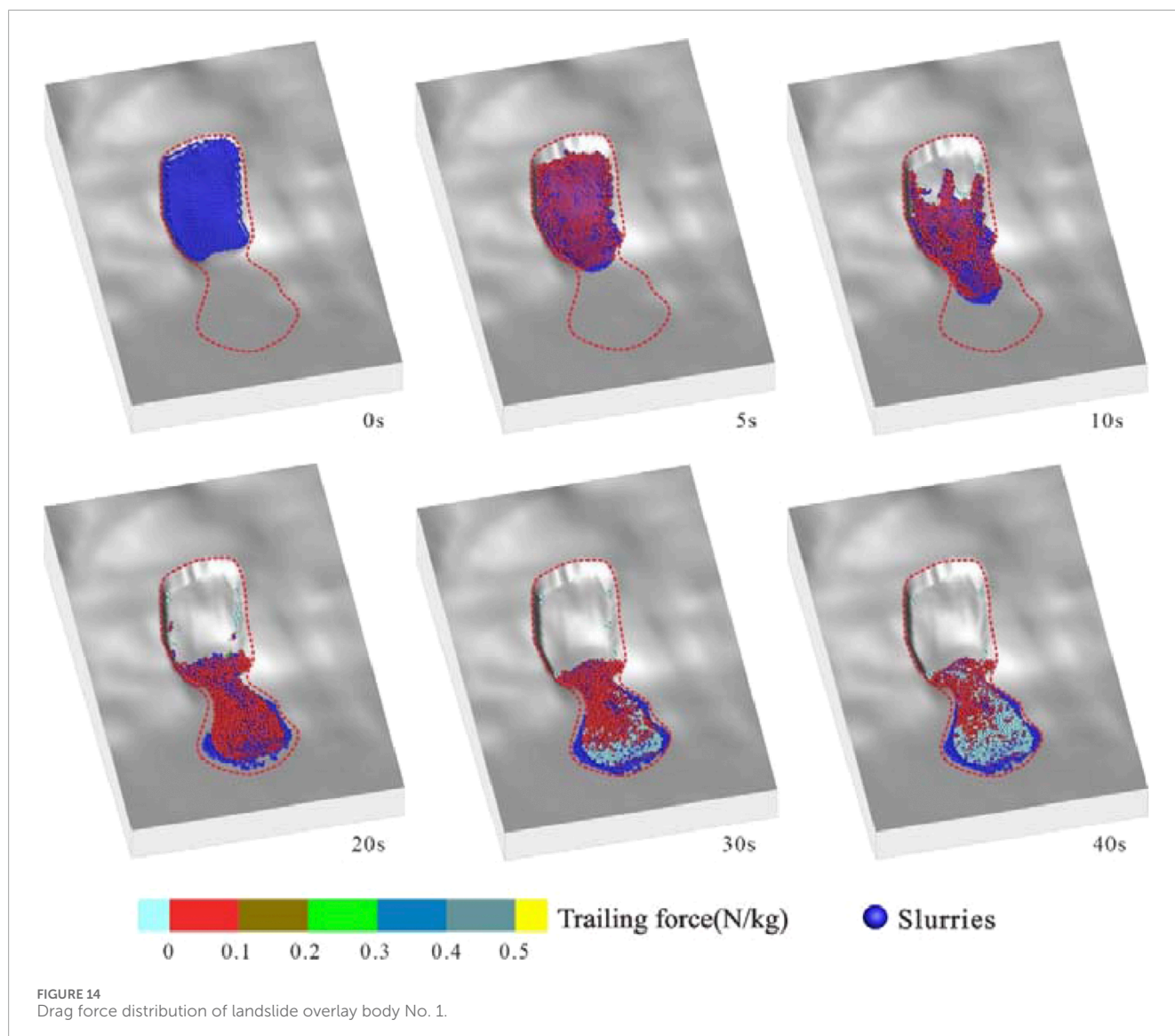
The results of the velocity simulation of the No.1~No.4 landslide overlay body are shown in Table 2, and the sliding process of No.4 landslide overlay body is the longest, lasting 70 s and reaching a peak velocity of 32.5 m/s (Figure 10), while the sliding process of No.3 landslide overlay body is the shortest, lasting only 30 s, with a peak velocity of 18.5 m/s (Figure 11). By analysing the key time points of the simulation process, it can be learnt that the solid particles of each landslide mixed with fluids and accelerated rapidly after initiation, and reached the peak velocity, and then decelerated gradually due to the limitation of geomorphological conditions until finally coming to a standstill.

#### 4.3.3 Analyses of simulation results on the accumulation of landslide overlay body

The simulation results of the accumulation thickness of the No.1~No.4 landslide overlay bodies are shown in Table 3, which are basically consistent with the results of the field investigation and have a high degree of agreement. Taking the simulation results of No.1 landslide overlay body as an example (Figure 12), the red dotted line marks the real landslide extent, while the changes of red, yellow and blue colours reflect the different dynamic changes of the accumulation thickness of solid particles. During the whole process of landslide movement, the rock and soil bodies mixed with mud flowed along the slope surface, and after energy dissipation, they eventually accumulated gradually at the foot of the slope, and the accumulation results were consistent with the actual landslide accumulation.

#### 4.3.4 Analysis of simulation results of volume fraction distribution of landslide overlay body

In order to distinguish the volume fraction of solid particles from the value of fluid volume fraction at each sliding stage, the volume fraction of solid particles is represented by a gradient colour

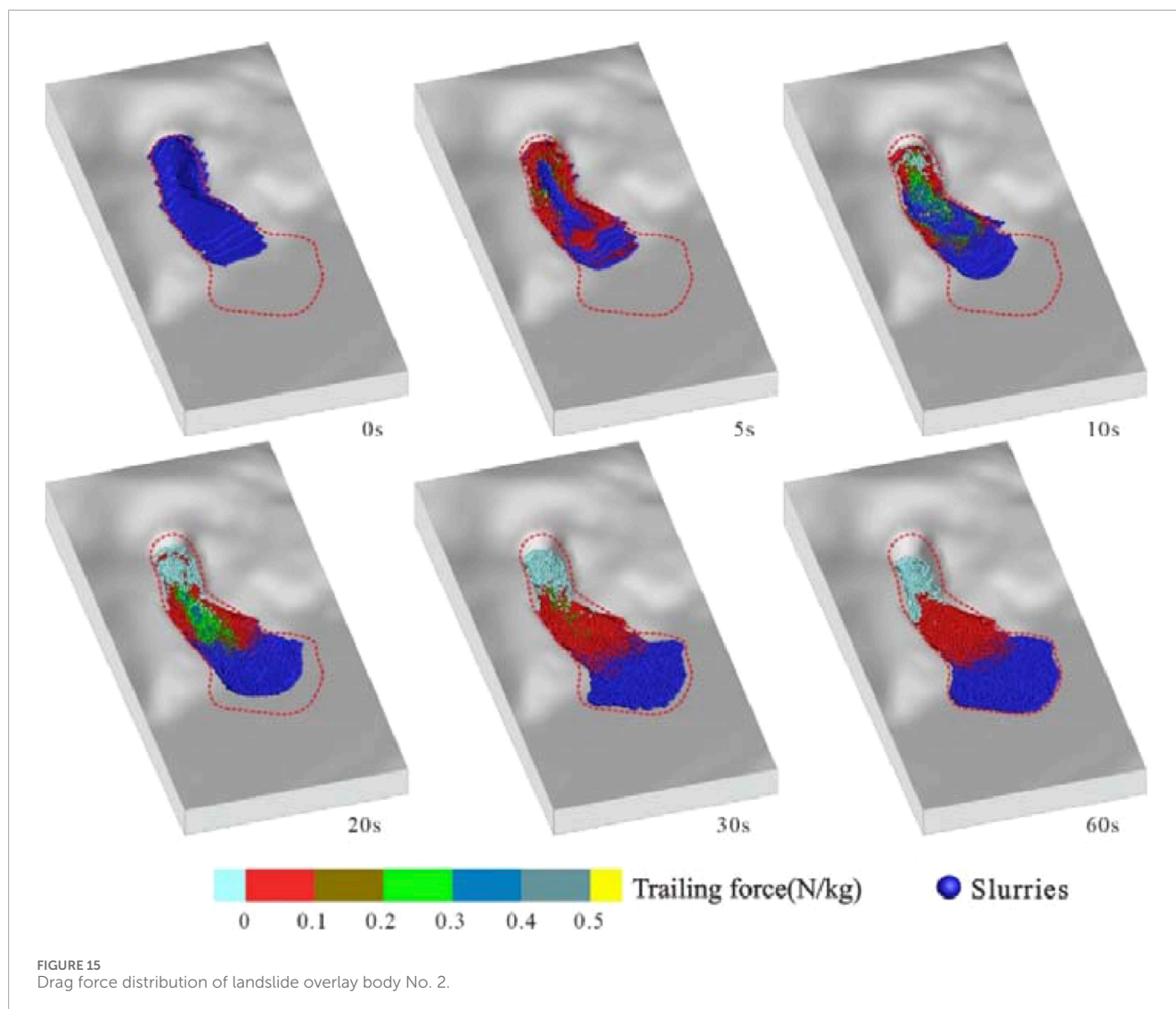


from red to yellow, while the fluid volume fraction is shown by a gradient colour from dark blue to light blue, and the sum of the two at each stage is 100%. As an example, the simulation results of landslide overlay body No. 1 (Figure 13) show that most of the solid particles are in a dense state with volume fractions between 60% and 80% due to the movement of the main body of landslide overlay body No. 1 along the slope. When at the outer edge of the landslide, no solid particles exist and only fluid is present, the fluid volume fraction reaches 100%.

#### 4.3.5 Analyses of simulation results of fluid drag force on the landslide overlay body

The simulation results of the fluid drag force of landslide overlay bodies No. 1~4 are shown in Figures 15–18, which demonstrate the distribution of the drag force per unit mass of fluid on solid particles of these four landslides at different time points, respectively. Since the initiation of the landslide motion, the solid particles are all under the action of the fluid with larger flow velocity and show the

fluidised motion characteristics along the gullies. During the motion of the four landslides, most of the solid particles were subjected to relatively small drag forces per unit mass, which are marked by the red areas, and their values were generally lower than 0.1 N/kg. However, the slides exhibited different characteristics in terms of drag force variations. For landslide overlay body No. 1 (Figure 14), the drag force per unit mass exerted on some solid particles exceeded 0.2 N/kg from 5 s. By 30 s, the drag force on some particles on the surface of the slip body dropped to 0 N/kg, indicating that the particles started to stop moving, and the movement stopped completely by 40 s. For landslide overlay body No. 2 (Figure 15), the drag force on some of the solid particles started to exceed 0.2 N/kg at about 8 s, and the drag force on a very few particles in the middle of the slide body reached 0.6 N/kg at about 10 s and 20 s, showing a trend of gradual increase in the difference between the flow and solid velocities, and the motion ceased after 60 s. The drag force of some particles in No.3 landslide overlay body (Figure 16) exceeded 0.2 N/kg from 10 s, and the drag force of some particles at the



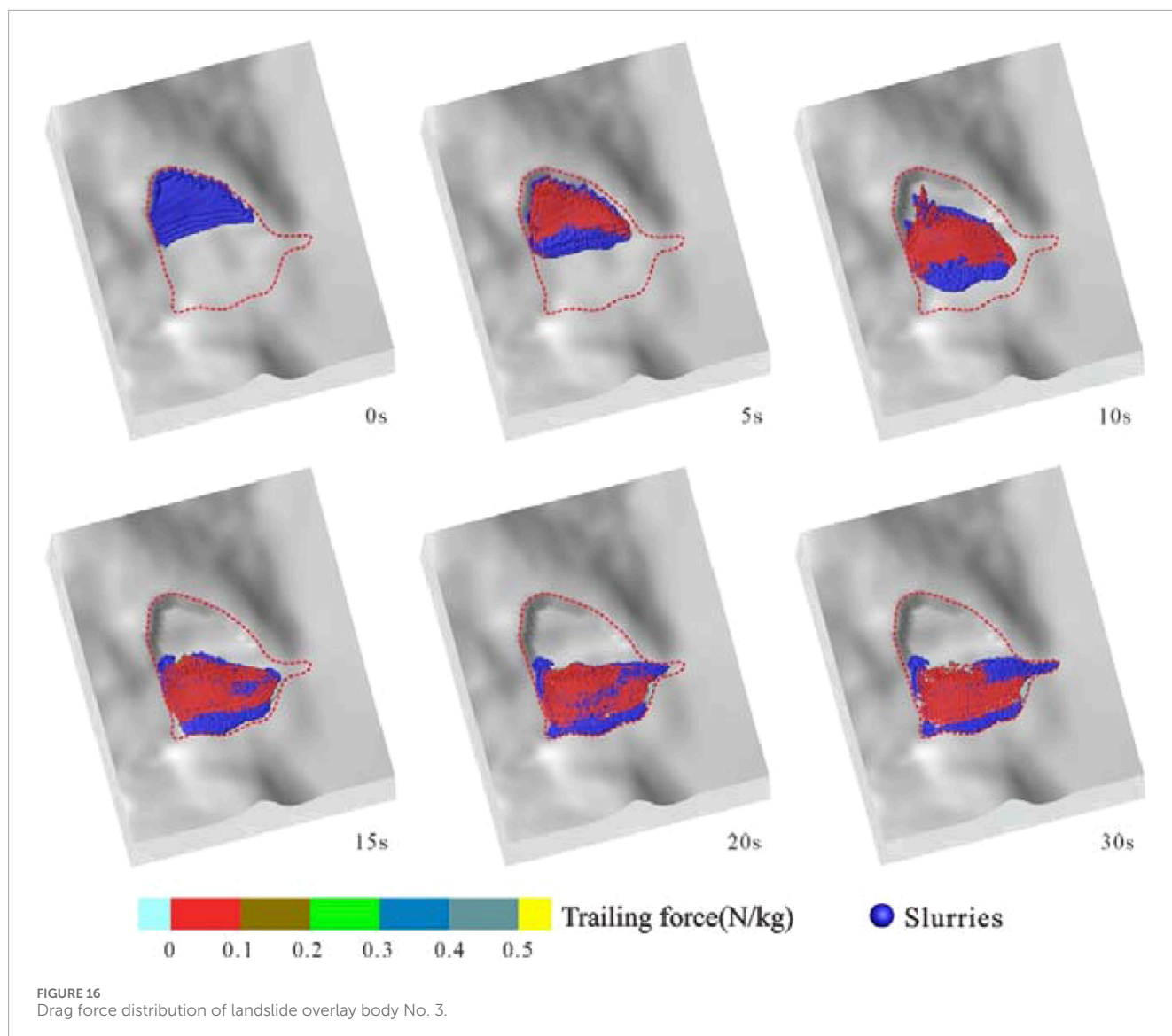
edge of the landslide overlay body was reduced to 0 N/kg after 15 s, and the motion was completely stopped at 30 s. The drag force of some particles in No.4 landslide overlay body (Figure 17) started to exceed 0.2 N/kg from 5 s, and the drag force of a few particles in the middle of the slide even reached more than 0.6 N/kg from 10 s to 30s, which indicated that the velocity difference between fluids and solids increased significantly, and the movement eventually stopped completely after 70 s.

In summary, all four landslides showed fluidised motion characteristics under the action of fluid drag force, but there were differences in the change characteristics of drag force and motion cessation time, and these results provide an important basis for further revealing the mechanism of landslide motion and predicting landslide disasters.

After summarising and analysing the simulation results of the four landslide overlay bodies in the Hongyacun landslide cluster, the final simulation stacking results can be derived as shown in Figure 18. According to the simulation data, the rock and soil body materials in the Hongyacun landslide cluster show a dense state in most areas. The maximum velocity of landslide

overlay body No.1 in the simulation reaches 22.4 m/s, the maximum thickness of the accumulation is 14 m, and the farthest distance of the slide reaches 300 m. Landslide overlay body No.2, the maximum velocity of the whole process reaches 21.8 m/s, the maximum thickness of the accumulation is 18.6 m, and the farthest distance of the slide reaches 480 m. Landslide overlay body No. 3 has a maximum velocity of 18.5 m/s, a maximum stacking thickness of 12 m, and a maximum distance of 200 m. Finally, landslide overlay body No. 4 has a maximum velocity of 32.5 m/s, a maximum stacking thickness of 10 m, and a maximum distance of 700 m.

In the simulation calculation process, the property parameters of the landslide materials are largely consistent with the actual situation, thereby ensuring the accuracy of the simulation results. Through comparative analysis, it is found that the simulation results are basically consistent with the actual accumulation of Hongyacun landslide cluster, which fully proves that the adopted simulation calculation method can effectively reflect the key role of rainfall conditions on the destabilisation of landslide clusters and their remote movement into disaster. This conclusion is of great significance for further understanding of the motion law



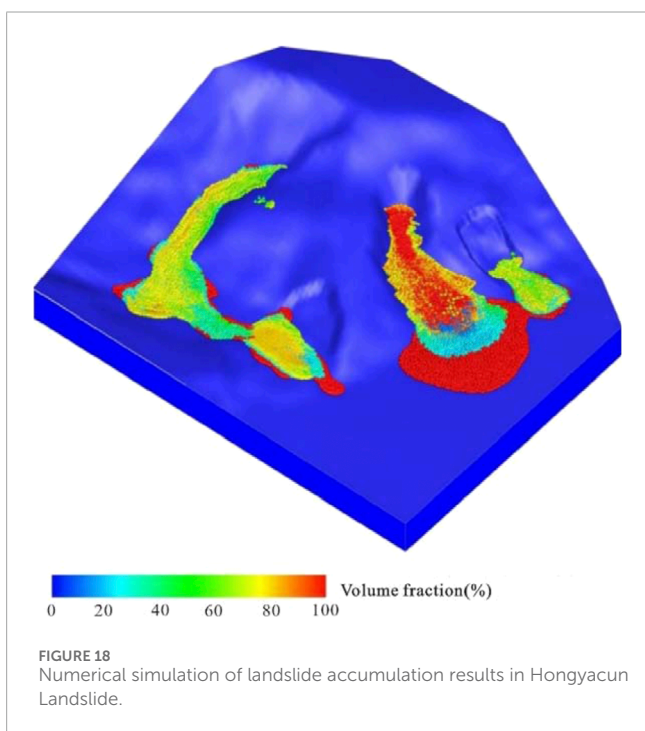
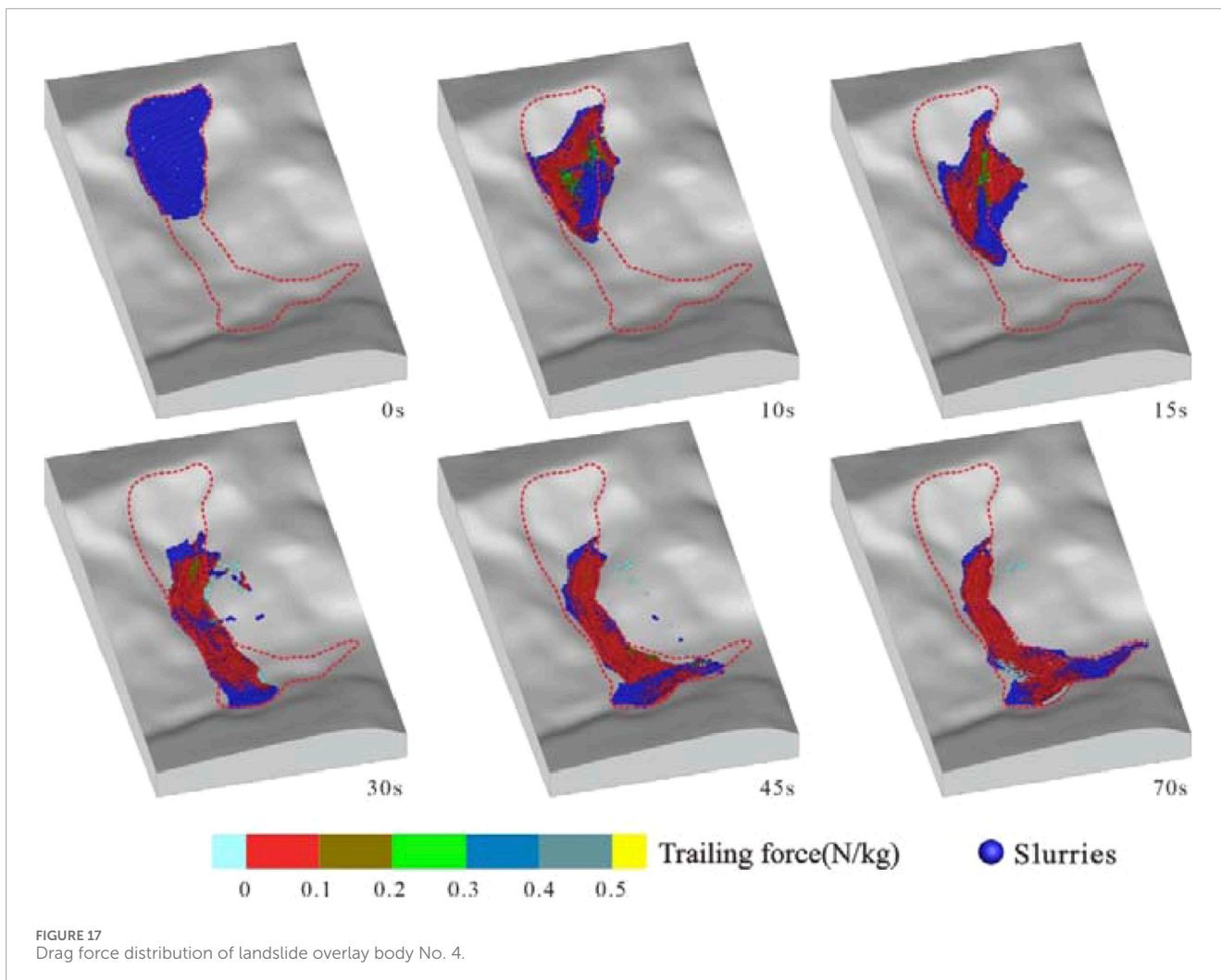
governing the Hongyacun landslide cluster and its catastrophic mechanism.

## 5 Discussion

In this study, the basic characteristics of the landslide cluster in Hongya Village, Qinghai were revealed in detail through field investigations. The investigation results show that the landslide cluster in Hongya Village mainly consists of two main landslides (H1 and H2), of which landslide H1 contains two sub-landslides (H1-1 and H1-2), and landslide H2 likewise contains two sub-landslides (H2-1 and H2-2). Each of these sub-landslides is characterised in terms of volume, distance travelled and deformation characteristics. For example, sub-slide H1-1 has a smaller volume and shorter travelling distance, whereas sub-slide H1-2 has experienced high-speed long-distance sliding due to the large height difference

between the front and back of the body and the high shear exit position. The back edge of landslide H2 has significant rock disintegration avalanches and slides, while the deformation volume of the middle and the front edges is small, and the developmental pattern and the number of the sub-slides are similar to that of the H1 landslide. These features not only provide us with the specific parameters of the landslides, but also demonstrate the different response modes of the landslides in the complex geological environment.

In terms of triggering mechanisms, the study analysed the influence of two major factors, geo-environmental and rainfall, on landslides. Geo-environmental factors include steep topography, weak interbedded layers, softening effect of groundwater on rock and soil, and anthropogenic slope-cutting activities, etc., which work together to cause landslide events. Rainfall is another key factor. Continuous heavy rainfall not only increases the self-weight of the soil, but also raises the water table, leading to a reduction in the shear strength of the slip surface, thus inducing landslides. In addition,



water leakage from landscaping and irrigation works on the surface of the landslide area exacerbates the risk of landslides.

Multiphase multimedimum numerical simulations using LPF3D software further revealed the dynamic behaviour of the landslides. The simulation results demonstrate the velocity of motion, volume fraction, stacking thickness, and drag force distribution during sliding for the four sub-slides under natural and rainfall conditions. The rainfall has a significant effect on the stability of the landslides, which leads to unstable sliding and exhibits fluidisation characteristics. The volume fraction of solid phase during movement of all sub-slides ranged from 60% to 80% and showed dense state characteristics. The fluid drag force of all the sub-slides gradually increased with the advancement of the slide motion, which indicated that the dynamic characteristics during the slide motion were complex and variable.

Under prolonged rainfall conditions, the continued infiltration of rainwater can have a significant impact on the stability of the loess layer, which in turn may induce landslide events and pose a serious safety threat to the neighbouring residential areas. In view of this, it is necessary to take a series of targeted measures during the rainy season in order to effectively mitigate the potential impacts of landslides on the lives and property safety of residents. Specifically, monitoring and early warning of extreme rainfall conditions should

be strengthened in Hongya Village to ensure that potential rainfall risks can be detected and responded to in a timely manner. At the same time, drainage facilities should be constructed and improved, with the aim of effectively directing the discharge of rainwater and preventing it from penetrating deep into the soil, thus avoiding the recurrence of landslides. Through the implementation of these comprehensive measures, the effectiveness of disaster prevention and mitigation can be significantly improved to ensure the safety of residents.

Although this study used LPF3D software to carry out an in-depth dynamic simulation and analysis of the landslide complex in Hongyacun, its limitations still need to be pointed out: although a multiphase multi-media simplification method was adopted during the model construction process, this simplification may fail to comprehensively reflect the real physical characteristics of the landslides, in particular the inhomogeneity of the landslide constituents and the complex rheological properties. Therefore, future research will be devoted to optimising the model parameters and improving the accuracy and applicability of the model in order to simulate the landslide motion process more accurately.

## 6 Conclusion

The Hongyacun landslide complex consists of two major landslides (H1 and H2), each of which contains two sub-landslides, each of which exhibits different characteristics in terms of volume, distance travelled and deformation characteristics.

The triggering mechanism of landslide clusters mainly involves two major factors, namely the geological environment and rainfall. Geo-environmental factors include steep topography, weak interbedded layers, softening effect of groundwater on rock and soil, and anthropogenic slope-cutting activities, while rainfall induces landslides by increasing the self-weight of the soil and raising the water table, which reduces the shear strength of the slip surface. In addition, water leakage from landscaping and irrigation works on the surface of landslide areas exacerbates the risk of landslides.

The multiphase multimedial numerical simulation using LPF3D software successfully reproduces the dynamic behaviour of the Hongyacun landslide cluster in the natural state and under the influence of rainfall. The simulation results reveal the influence of rainfall on the stability of the landslide, and indicate that rainfall can lead to the unstable sliding of the landslide, and the unstable soil body exhibits significant fluidisation characteristics. Among the four sub-landslides, landslide H2-2 has the longest duration of movement, the highest velocity, and the farthest distance of movement, which is about 700 m. These conclusions provide an important scientific basis for early warning and prevention of landslide disasters.

The continuous infiltration of rainwater caused by prolonged rainfall significantly affects the stability of the loess layer, inducing landslide events and posing a serious safety threat to the neighbouring residential areas of Hongya Village. Therefore, strengthening the monitoring and early warning of extreme rainfall during the rainy season and constructing and improving drainage facilities to prevent rainwater from penetrating deeper into the soil are effective measures to mitigate landslide disasters and ensure the safety of residents.

## Data availability statement

The raw data supporting the conclusions of this article will be made available by the authors, without undue reservation.

## Author contributions

GW: Conceptualization, Data curation, Investigation, Methodology, Software, Writing–original draft. ZX: Data curation, Investigation, Project administration, Software, Writing–review and editing. JY: Conceptualization, Formal Analysis, Methodology, Resources, Software, Writing–review and editing. BL: Data curation, Methodology, Writing–review and editing. XW: Data curation, Resources, Writing–review and editing.

## Funding

The author(s) declare that financial support was received for the research, authorship, and/or publication of this article. This work was supported by Science and Technology Project of Qinghai 906 Engineering Survey and Design Institute (no. 2023-KJ-06), the Top Talents Program for High-End Innovative Talents in Qinghai Province (No. 2021-12), and the Scientific Research Projects of the Chinese Academy of Geological Sciences (HX2023-21).

## Acknowledgments

The authors express their gratitude to Prof. Yang Gao for supplying a copy of the LPF3D software.

## Conflict of interest

The authors declare that the research was conducted in the absence of any commercial or financial relationships that could be construed as a potential conflict of interest.

## Generative AI statement

The author(s) declare that no Generative AI was used in the creation of this manuscript.

## Publisher's note

All claims expressed in this article are solely those of the authors and do not necessarily represent those of their affiliated organizations, or those of the publisher, the editors and the reviewers. Any product that may be evaluated in this article, or claim that may be made by its manufacturer, is not guaranteed or endorsed by the publisher.

## References

- Chen, H., and Lee, C. F. (2003). A dynamic model for rainfall-induced landslides on natural slopes. *Geomorphology* 51 (4), 269–288. doi:10.1016/s0169-555x(02)00224-6
- Crosta, G. B., Imposimato, S., and Roddeman, D. G. (2003). Numerical modelling of large landslides stability and runout. *Nat. Hazards Earth Syst. Sci.* 3 (6), 523–538. doi:10.5194/nhess-3-523-2003
- Davies, T. R., and McSaveney, M. J. (1999). Runout of dry granular avalanches. *Can. Geotech. J.* 36, 313–320. doi:10.1139/t98-108
- Denlinger, R. P., and Iverson, R. M. (2004). Granular avalanches across irregular three-dimensional terrain: 1. Theory and computation. *J. Geophys. Res. Earth Surf.* 109 (F1), 1–14. doi:10.1029/2003jf000085
- Gao, Y., Li, B., Zhang, H., Wu, W., Li, J., and Yin, Y. (2024b). Numerical modeling of mixed two-phase in long runout flow-like landslide using LPP3D. *Landslides* 21 (3), 641–660. doi:10.1007/s10346-023-02159-8
- Gao, Y., Yin, Y., Li, B., Feng, Z., Wang, W., Zhang, N., et al. (2017). Characteristics and numerical runout modeling of the heavy rainfall-induced catastrophic landslide–debris flow at Sanxicun, Dujiangyan, China, following the Wenchuan Ms 8.0 earthquake. *Landslides* 14, 1361–1374. doi:10.1007/s10346-016-0793-4
- Gao, Y., Yin, Y., Li, B., Wei, T., Li, Z., and Gao, H. (2022). The role of fluid drag force in the dynamic process of two-phase flow-like landslides. *Landslides* 19, 1791–1805. doi:10.1007/s10346-022-01858-y
- Gao, Y., Yin, Y., Li, B., Zhang, H., Wu, W., and Gao, H. (2024a). Multistate transition and coupled solid–liquid modeling of motion process of long-runout landslide. *J. Rock Mech. Geotechnical Eng.* 16 (7), 2694–2714. doi:10.1016/j.jrmge.2023.12.001
- Gao, Y., Yin, Y. P., Li, B., Wang, B. X., and Xiao, H. (2023). A numerical simulation method for high-level remote landslides considering particle state transformation. *J. Rock Mech. Eng.* 42 (7), 1623–1637.
- He, Q., Guo, F. Y., Li, R. D., Wang, L., Wang, W., Zhang, N., et al. (2023). Characteristics, mobility and dynamic of the Yahuokou flow-like landslide in Zhouqu, Gansu, China. *Gansu, China. Landslides* 20, 629–643. doi:10.1007/s10346-022-02000-8
- He, Q., Wang, Y., Wang, W. P., Xu, W., Zhao, G., Chen, L., et al. (2024). Mechanism of the November 2018 landslide at the Kunming landfill and the geotechnical engineering risk control in the process of urbanization. *Bull. Eng. Geol. Environ.* 83, 196. doi:10.1007/s10064-024-03703-z
- Huang, Y., Zhang, W. J., Xu, Q., Xie, P., and Hao, L. (2012). Run-out analysis of flow-like landslides triggered by the Ms 8.0 2008 Wenchuan earthquake using smoothed particle hydrodynamics. *Landslides* 9 (2), 275–283. doi:10.1007/s10346-011-0285-5
- Hung, O. (1995). A model for the runout analysis of rapid flow slides, debris flows, and avalanches. *Can. Geotech. J.* 32 (4), 610–623. doi:10.1139/t95-063
- Hung, O. (2008). Simplified models of spreading flow of dry granular material. *Can. Geotech. J.* 45 (8), 1156–1168. doi:10.1139/t08-059
- Hung, O., and Evans, S. G. (2004). Entrainment of debris in rock avalanches: an analysis of a long-runout mechanism. *Geol. Soc. Am. Bull.* 116, 1240–1252. doi:10.1130/b25362.1
- Liu, W., He, S. M., Li, X. B., and Xu, Q. (2015). Two-dimensional landslide dynamic simulation based on a velocity-weakening friction law. *Landslides* 13 (5), 957–965. doi:10.1007/s10346-015-0632-z
- McDougall, S., and Hung, O. (2004). A model for the analysis of rapid landslide motion across three-dimensional terrain. *Can. Geotech. J.* 41 (6), 1084–1097. doi:10.1139/t04-052
- Pastor, M., Blanc, T., Haddad, B., Petrone, S., Sanchez Morles, M., Dremptic, V., et al. (2014). Application of a SPH depth-integrated model to landslide run-out analysis. *Landslides* 11, 793–812. doi:10.1007/s10346-014-0484-y
- Pirulli, M., and Mangeney, A. (2008). Results of back-analysis of the propagation of rock avalanches as a function of the assumed rheology. *Rock Mech. Rock Eng.* 41 (1), 59–84. doi:10.1007/s00603-007-0143-x
- Poisel, R., Preh, A., and Hung, O. (2008). Run out of landslides-continuum mechanics versus discontinuum mechanics models. *Geomech. Tunn.* 1 (5), 358–366. doi:10.1002/geot.200800036
- Pudasaini, S. P., and Miller, S. A. (2013). The hypermobility of huge landslides and avalanches. *Eng. Geol.* 157, 124–132. doi:10.1016/j.enggeo.2013.01.012
- Sassa, K. (1988). Geotechnical model for the motion of landslides. *Proc. 5th Int. Symposium Landslides* 1, 37–56.
- Sassa, K., Nagai, O., Solidum, R., Yamazaki, Y., and Ohta, H. (2010). An integrated model simulating the initiation and motion of earthquake and rain induced rapid landslides and its application to the 2006 Leyte landslide. *Landslides* 7 (3), 219–236. doi:10.1007/s10346-010-0230-z
- Tang, C., Zhu, J., Ding, J., Cui, X. F., Chen, L., and Zhang, J. S. (2011). Catastrophic debris flows triggered by a 14 August 2010 rainfall at the epicenter of the Wenchuan earthquake. *Landslides* 8, 485–497. doi:10.1007/s10346-011-0269-5
- Wang, Y., He, Q., Wang, W., Zhang, N., Chen, L., Liu, Z., et al. (2024). Analysis on the mechanism and dynamics of frequent debris flows in typical alpine gorges areas—a case study of Yizhong river in Deqin County, Yunnan, China. *Front. Earth Sci.* 12, 1418763. doi:10.3389/feart.2024.1418763
- Xing, A. G., Wang, G. H., Li, B., Jiang, Y., Feng, Z., and Kamai, T. (2015). Long-runout mechanism and landslide behaviour of large catastrophic landslide triggered by heavy rainfall in Guanling, Guizhou, China. *Can. Geotech. J.* 52 (7), 971–981. doi:10.1139/cgj-2014-0122
- Xu, Q., Fan, X. M., and Dong, X. J. (2010). Characteristics and formation mechanism of a catastrophic rainfall-induced rock avalanche–mud flow in Sichuan, China. *Landslides* 9, 143–154. doi:10.1007/s10346-011-0278-4
- Yan, J., Ma, Y., Liu, L., Wang, Z., and Ren, T. (2024). Numerical simulation of rainfall-induced xianchi reservoir landslide in yunyang, chongqing, China. *Acta Geol. Sin. Engl. Ed.* 98 (2), 505–517. doi:10.1111/1755-6724.15146
- Yin, Y. P., Cheng, Y. L., Liang, J. T., and Wang, W. P. (2016). Heavy-rainfall-induced catastrophic rockslide - debris flow at Sanxicun, Dujiangyan, after the Wenchuan Ms 8.0 earthquake. *Landslides* 13, 9–23. doi:10.1007/s10346-015-0554-9
- Yin, Y. P., Sun, P., Zhu, J. L., and Yang, S. Y. (2011). Research on catastrophic rock avalanche at Guanling, Guizhou, China. *Landslides* 8 (4), 517–525. doi:10.1007/s10346-011-0266-8
- Yin, Y. P., Xing, A. G., Wang, G. H., Feng, Z., Li, B., and Jiang, Y. (2017). Experimental and numerical investigations of a catastrophic long-runout landslide in Zhenxiang, Yunnan, southwestern China. *Landslides* 14, 649–659. doi:10.1007/s10346-016-0729-z
- Zhang, M., Yin, Y. P., and Wu, S. R. (2010). Development status and prospects of studies on kinematics of long runout rock avalanches. *J. Eng. Geol.* 18 (6), 805–817.
- Zhang, S. L., Yin, Y. P., Hu, X. W., Wang, W. P., Zhang, N., Zhu, S. N., et al. (2020). Dynamics and emplacement mechanisms of the successive baige landslides on the upper reaches of the jinsha river, China. *Eng. Geol.* 278 (1), 105819. doi:10.1016/j.enggeo.2020.105819
- Zhang, T., Gao, Y., Li, B., Yin, Y., Liu, X., Gao, H., et al. (2023). Characteristics of rock-ice avalanches and geohazard-chains in the parlung zangbo basin, tibet, China. *Geomorphology* 422, 108549. doi:10.1016/j.geomorph.2022.108549